

000 054
 001 055
 002 056
 003 057
 004 058
 005 059
 006 060
 007 061
 008 062
 009 063
 010 064
 011 065
 012 066
 013 067
 014 068
 015 069
 016 070
 017 071
 018 072
 019 073
 020 074
 021 075
 022 076
 023 077
 024 078
 025 079
 026 080
 027 081
 028 082
 029 083
 030 084
 031 085
 032 086
 033 087
 034 088
 035 089
 036 090
 037 091
 038 092
 039 093
 040 094
 041 095
 042 096
 043 097
 044 098
 045 099
 046 100
 047 101
 048 102
 049 103
 050 104
 051 105
 052 106
 053 107

Supplementary File to “Multi-channel Weighted Nuclear Norm Minimization for Real Color Image Denoising”

Anonymous ICCV submission

Paper ID 572

In this supplementary file, we provide:

1. The proof of the Theorem 1 in the main paper.
2. More denoising results on the 24 high quality images from the Kodak PhotoCD dataset.
3. More visual comparisons of denoised images by different methods on the real noisy images of the dataset [1].
4. More visual comparisons of denoised images by different methods on the real noisy images of the dataset [2].

1. Proof of Theorem 1.

Theorem 1. Assume that the weights in w are in a non-descending order, the sequence $\{\mathbf{X}_k\}$, $\{\mathbf{Z}_k\}$, and $\{\mathbf{A}_k\}$ generated in Algorithm 1 satisfy:

$$(a) \lim_{k \rightarrow \infty} \|\mathbf{X}_{k+1} - \mathbf{Z}_{k+1}\|_F = 0; \quad (b) \lim_{k \rightarrow \infty} \|\mathbf{X}_{k+1} - \mathbf{X}_k\|_F = 0; \quad (c) \lim_{k \rightarrow \infty} \|\mathbf{Z}_{k+1} - \mathbf{Z}_k\|_F = 0. \quad (1)$$

Proof. 1. Firstly, we prove that the sequence $\{\mathbf{A}_k\}$ generated by Algorithm 1 is upper bounded. Let $\mathbf{X}_{k+1} + \rho_k^{-1} \mathbf{A}_k = \mathbf{U}_k \Sigma_k \mathbf{V}_k^\top$ be its singular value decomposition (SVD) [3] in the $(k+1)$ -th iteration. According to Corollary 1 of [4], we can have the SVD of \mathbf{Z}_{k+1} as $\mathbf{Z}_{k+1} = \mathbf{U}_k \hat{\Sigma}_k \mathbf{V}_k^\top = \mathbf{U}_k \mathcal{S}_{\frac{w}{\rho_k}}(\Sigma_k) \mathbf{V}_k^\top$. Then we have

$$\|\mathbf{A}_{k+1}\|_F = \|\mathbf{A}_k + \rho_k(\mathbf{X}_{k+1} - \mathbf{Z}_{k+1})\|_F = \rho_k \|\rho_k^{-1} \mathbf{A}_k + \mathbf{X}_{k+1} - \mathbf{Z}_{k+1}\|_F \quad (2)$$

$$= \rho_k \|\mathbf{U}_k \Sigma_k \mathbf{V}_k^\top - \mathbf{U}_k \mathcal{S}_{\frac{w}{\rho_k}}(\Sigma_k) \mathbf{V}_k^\top\|_F = \rho_k \|\Sigma_k - \mathcal{S}_{\frac{w}{\rho_k}}(\Sigma_k)\|_F \quad (3)$$

$$= \rho_k \sqrt{\sum_i (\Sigma_k^{ii} - \mathcal{S}_{\frac{w}{\rho_k}}(\Sigma_k^{ii}))^2} \leq \rho_k \sqrt{\sum_i \left(\frac{w_i}{\rho_k}\right)^2} = \sqrt{\sum_i w_i^2}. \quad (4)$$

The inequality in the second last step can be proved as follows: given the diagonal matrix Σ_k , we define Σ_k^{ii} as the i -th element of Σ_k^{ii} . If $\Sigma_k^{ii} \geq \frac{w_i}{\rho_k}$, we have $\mathcal{S}_{\frac{w}{\rho_k}}(\Sigma_k^{ii}) = \Sigma_k^{ii} - \frac{w_i}{\rho_k} \geq 0$. If $\Sigma_k^{ii} < \frac{w_i}{\rho_k}$, we have $\mathcal{S}_{\frac{w}{\rho_k}}(\Sigma_k^{ii}) = 0 < \Sigma_k^{ii} + \frac{w_i}{\rho_k}$. After all, we have $|\Sigma_k^{ii} - \mathcal{S}_{\frac{w}{\rho_k}}(\Sigma_k^{ii})| \leq \frac{w_i}{\rho_k}$ and hence the inequality holds true. Hence, the sequence $\{\mathbf{A}_k\}$ is upper bounded.

2. Secondly, we prove that the sequence of Lagrangian function $\{\mathcal{L}(\mathbf{X}_{k+1}, \mathbf{Z}_{k+1}, \mathbf{A}_k, \rho_k)\}$ is also upper bounded. Since the global optimal solution of \mathbf{X} and \mathbf{Z} in corresponding subproblems, we always have $\mathcal{L}(\mathbf{X}_{k+1}, \mathbf{Z}_{k+1}, \mathbf{A}_k, \rho_k) \leq \mathcal{L}(\mathbf{X}_k, \mathbf{Z}_k, \mathbf{A}_k, \rho_k)$. Based on the updating rule that $\mathbf{A}_{k+1} = \mathbf{A}_k + \rho_k(\mathbf{X}_{k+1} - \mathbf{Z}_{k+1})$, we have $\mathcal{L}(\mathbf{X}_{k+1}, \mathbf{Z}_{k+1}, \mathbf{A}_{k+1}, \rho_{k+1}) = \mathcal{L}(\mathbf{X}_{k+1}, \mathbf{Z}_{k+1}, \mathbf{A}_k, \rho_k) + \langle \mathbf{A}_{k+1} - \mathbf{A}_k, \mathbf{X}_{k+1} - \mathbf{Z}_{k+1} \rangle + \frac{\rho_{k+1} - \rho_k}{2} \|\mathbf{X}_{k+1} - \mathbf{Z}_{k+1}\|_F^2 = \mathcal{L}(\mathbf{X}_{k+1}, \mathbf{Z}_{k+1}, \mathbf{A}_k, \rho_k) + \frac{\rho_{k+1} + \rho_k}{2\rho_k^2} \|\mathbf{A}_{k+1} - \mathbf{A}_k\|_F^2$. Since the sequence $\{\|\mathbf{A}_k\|\}$ is upper bounded, the sequence $\{\|\mathbf{A}_{k+1} - \mathbf{A}_k\|_F\}$ is also upper bounded. Denote by a the upper bound of $\{\|\mathbf{A}_{k+1} - \mathbf{A}_k\|_F\}$, we have $\mathcal{L}(\mathbf{X}_{k+1}, \mathbf{Z}_{k+1}, \mathbf{A}_{k+1}, \rho_{k+1}) \leq \mathcal{L}(\mathbf{X}_1, \mathbf{Z}_1, \mathbf{A}_0, \rho_0) + a \sum_{k=0}^{\infty} \frac{\rho_{k+1} + \rho_k}{2\rho_k^2} = \mathcal{L}(\mathbf{X}_1, \mathbf{Z}_1, \mathbf{A}_0, \rho_0) + a \sum_{k=0}^{\infty} \frac{\mu+1}{2\mu^k \rho_0} \leq \mathcal{L}(\mathbf{X}_1, \mathbf{Z}_1, \mathbf{A}_0, \rho_0) + \frac{a}{\rho_0} \sum_{k=0}^{\infty} \frac{1}{\mu^{k-1}}$. The last inequality holds since $\mu+1 < 2\mu$. Since $\sum_{k=0}^{\infty} \frac{1}{\mu^{k-1}} < \infty$, the sequence of Lagrangian function $\{\mathcal{L}(\mathbf{X}_{k+1}, \mathbf{Z}_{k+1}, \mathbf{A}_{k+1}, \rho_{k+1})\}$ is upper bound.

3. Thirdly, we prove that the sequences of $\{\mathbf{X}_k\}$ and $\{\mathbf{Z}_k\}$ are upper bounded. Since $\|\mathbf{W}(\mathbf{Y} - \mathbf{X})\|_F^2 + \|\mathbf{Z}\|_{w,*} = \mathcal{L}(\mathbf{X}_k, \mathbf{Z}_k, \mathbf{A}_{k-1}, \rho_{k-1}) - \langle \mathbf{A}_k, \mathbf{X}_k - \mathbf{Z}_k \rangle - \frac{\rho_k}{2} \|\mathbf{X}_k - \mathbf{Z}_k\|_F^2 = \mathcal{L}(\mathbf{X}_k, \mathbf{Z}_k, \mathbf{A}_{k-1}, \rho_{k-1}) + \frac{1}{2\rho_k} (\|\mathbf{A}_{k-1}\|_F^2 - \|\mathbf{A}_k\|_F^2)$. Thus $\{\mathbf{W}(\mathbf{Y} - \mathbf{X}_k)\}$ and $\{\mathbf{Z}_k\}$ are upper bounded, and hence the sequence $\{\mathbf{X}_k\}$ is bounded by the Cauchy-Schwarz inequality

Table 1. PSNR(dB) results of different denoising methods on 24 natural images.

Image#	$\sigma_r = 5, \sigma_g = 30, \sigma_b = 15$								
	CBM3D	MLP	TNRD	NI	NC	WNNM-1	WNNM-2	WNNM-3	MC-WNNM
1	27.25	28.06	28.62	25.00	29.55	28.16	27.95	28.15	30.20
2	29.70	31.30	32.70	27.80	29.69	32.54	31.60	31.73	34.04
3	30.34	31.98	34.07	28.02	31.93	33.91	33.68	33.52	35.55
4	29.47	31.10	32.56	27.70	32.56	32.68	31.85	31.90	34.06
5	27.31	28.59	29.35	26.14	30.00	28.83	29.00	28.91	30.05
6	28.20	29.10	29.90	26.15	28.81	29.55	29.46	29.62	31.64
7	29.73	31.60	33.46	27.22	31.63	33.09	33.29	32.86	34.24
8	27.47	28.16	28.91	25.34	30.16	29.15	29.24	29.03	29.91
9	30.07	31.63	33.55	27.86	31.54	33.19	33.20	32.95	34.53
10	29.96	31.37	33.20	27.74	33.44	32.98	33.02	32.74	34.38
11	28.73	29.85	30.87	26.98	30.16	30.45	30.14	30.21	32.10
12	30.20	31.50	33.31	27.97	31.69	33.22	32.71	32.65	34.64
13	26.18	26.69	26.98	25.14	27.97	26.49	26.42	26.62	28.30
14	27.86	29.07	29.87	26.67	29.21	29.36	29.14	29.30	31.18
15	29.91	31.58	33.13	28.04	31.17	33.22	32.34	32.36	34.27
16	29.29	30.35	31.54	27.46	32.18	31.34	31.05	31.21	33.72
17	29.50	31.09	32.52	27.81	32.80	32.09	32.00	31.85	33.61
18	27.72	28.74	29.36	26.57	28.63	28.88	28.76	28.89	30.56
19	28.98	30.18	31.35	27.25	29.79	31.34	30.77	30.95	33.10
20	30.63	31.78	33.27	27.89	29.52	33.00	32.55	32.58	34.18
21	28.50	29.58	30.54	26.86	30.99	30.02	30.03	30.03	31.69
22	28.61	29.78	30.82	27.19	30.50	30.47	29.82	30.10	32.08
23	30.60	32.66	35.06	28.17	32.82	34.72	34.37	33.94	35.16
24	27.97	28.81	29.61	26.01	30.75	29.47	29.35	29.39	30.93
Average	28.92	30.19	31.44	27.04	30.73	31.17	30.91	30.89	32.67

and triangle inequality. We can obtain that $\lim_{k \rightarrow \infty} \|\mathbf{X}_{k+1} - \mathbf{Z}_{k+1}\|_F = \lim_{k \rightarrow \infty} \rho_k^{-1} \|\mathbf{A}_{k+1} - \mathbf{A}_k\|_F = 0$ and the equation (a) is proved.

4. Then we can prove that $\lim_{k \rightarrow \infty} \|\mathbf{X}_{k+1} - \mathbf{X}_k\|_F = \lim_{k \rightarrow \infty} \|(\mathbf{W}^\top \mathbf{W} + \frac{\rho_k}{2} \mathbf{I})^{-1} (\mathbf{W}^\top \mathbf{W} \mathbf{Y} - \mathbf{W}^\top \mathbf{W} \mathbf{Z}_k - \frac{1}{2} \mathbf{A}_k) - \rho_k^{-1} (\mathbf{A}_k - \mathbf{A}_{k-1})\|_F \leq \lim_{k \rightarrow \infty} \|(\mathbf{W}^\top \mathbf{W} + \frac{\rho_k}{2} \mathbf{I})^{-1} (\mathbf{W}^\top \mathbf{W} \mathbf{Y} - \mathbf{W}^\top \mathbf{W} \mathbf{Z}_k - \frac{1}{2} \mathbf{A}_k)\|_F + \rho_k^{-1} \|\mathbf{A}_k - \mathbf{A}_{k-1}\|_F = 0$ and hence (b) is proved.

5. Finally, (c) can be proved by checking that $\lim_{k \rightarrow \infty} \|\mathbf{Z}_{k+1} - \mathbf{Z}_k\|_F = \lim_{k \rightarrow \infty} \|\mathbf{X}_k + \rho_k^{-1} \mathbf{A}_{k-1} - \mathbf{Z}_k + \mathbf{X}_{k+1} - \mathbf{X}_k + \rho_k^{-1} \mathbf{A}_{k-1} + \rho_k^{-1} \mathbf{A}_k - \rho_k^{-1} \mathbf{A}_{k+1}\|_F \leq \lim_{k \rightarrow \infty} \|\Sigma_{k-1} - \mathcal{S}_{w/\rho_{k-1}}(\Sigma_{k-1})\|_F + \|\mathbf{X}_{k+1} - \mathbf{X}_k\|_F + \rho_k^{-1} \|\mathbf{A}_{k-1} + \mathbf{A}_{k+1} - \mathbf{A}_k\|_F = 0$, where $\mathbf{U}_{k-1} \Sigma_{k-1} \mathbf{V}_{k-1}^\top$ is the SVD of the matrix $\mathbf{X}_k + \rho_{k-1} \mathbf{A}_{k-1}$. \square

2. More denoising results on the 24 high quality images from the Kodak PhotoCD dataset

In the main paper, we have given the PSNR results of the competing methods on the 24 high quality images from the Kodak PhotoCD dataset when the standard deviations of the additive white Gaussian noise (AWGN) are $\sigma_r = 40, \sigma_g = 20, \sigma_b = 30$ for R, G, B channels, respectively. Here we provide more denoising results on this dataset. In Tables ??-??, we give more PSNR results on these images when the noise standard deviations are $\sigma_r = 5, \sigma_g = 30, \sigma_b = 15$ in Table 1 and $\sigma_r = 30, \sigma_g = 10, \sigma_b = 50$ in Table 2, respectively. In Figures 7-??, we give the visual comparisons of the denoised images by different methods.

216

217

218

219

220

221

222

223

224

225

226

227

228

229

230

231

232

233

234

235

236

237

238

239

240

241

242

243

244

245

246

247

248

249

250

251

252

253

254

255

256

257

258

259

260

261

262

263

264

265

266

267

268

269

270

271

272

273

274

275

276

277

278

279

280

281

282

283

284

285

286

287

288

289

290

291

292

293

294

295

296

297

298

299

300

301

302

303

304

305

306

307

308

309

310

311

312

313

314

315

316

317

318

319

320

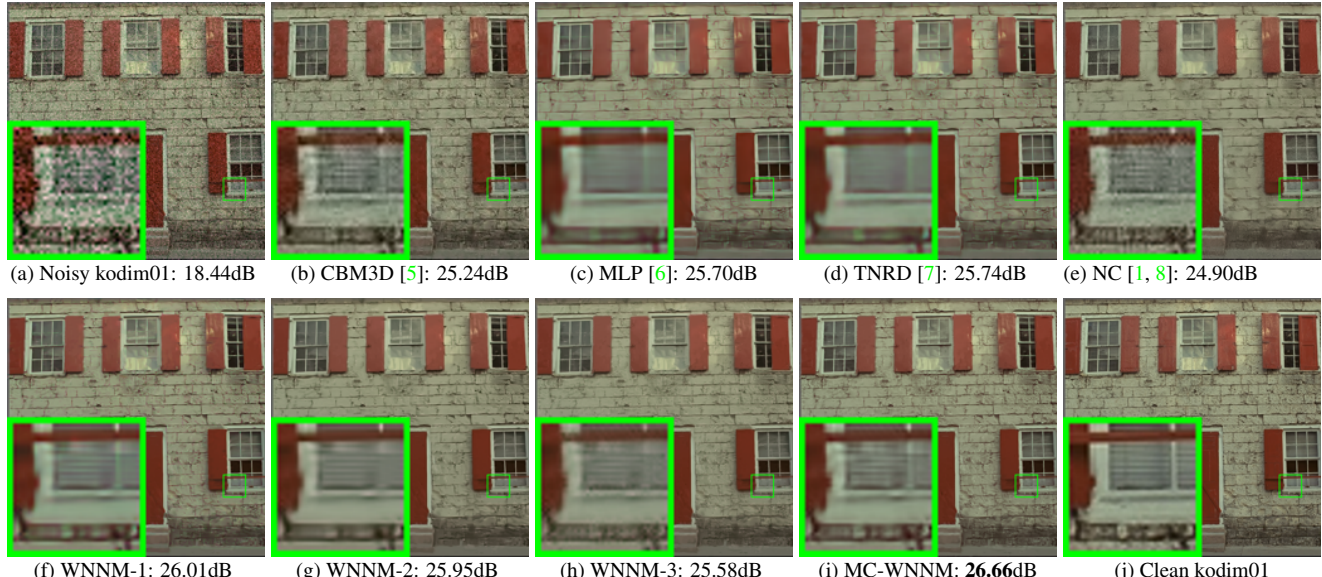
321

322

323

Table 2. PSNR(dB) results of different denoising methods on 24 natural images.

Image#	CBM3D	MLP	TNRD	NI	NC	WNNM-1	WNNM-2	WNNM-3	MC-WNNM
1	23.38	26.49	26.50	24.82	23.59	26.40	25.60	24.76	27.81
2	25.19	30.94	30.90	26.82	27.79	30.89	29.75	29.21	30.96
3	25.39	32.03	32.09	27.52	27.41	32.20	31.17	30.39	32.89
4	24.96	30.55	30.47	27.34	27.00	30.74	29.71	29.10	31.19
5	23.29	26.65	26.73	25.72	26.67	26.74	25.98	24.68	27.60
6	24.09	27.76	27.70	26.10	26.12	27.85	26.96	26.01	29.15
7	24.89	30.70	30.72	27.17	28.07	30.91	29.94	28.87	31.37
8	23.30	26.12	26.27	25.59	26.11	26.87	26.33	24.74	27.44
9	25.20	31.35	31.31	27.74	28.33	31.30	30.45	29.44	32.08
10	25.13	31.01	31.05	27.60	28.53	31.12	30.17	29.21	31.83
11	24.54	28.79	28.82	26.72	24.40	28.73	27.79	26.94	29.60
12	25.43	31.60	31.60	27.82	29.01	31.59	30.62	29.91	32.11
13	22.50	24.71	24.73	24.96	23.36	24.70	23.85	22.86	25.96
14	23.91	27.69	27.72	26.26	23.08	27.62	26.81	25.91	28.57
15	25.45	31.09	31.05	27.36	28.49	31.29	30.21	29.46	31.39
16	24.89	29.79	29.73	27.35	27.10	29.84	28.85	28.13	31.10
17	25.12	30.26	30.24	27.15	27.54	30.11	29.35	28.43	31.08
18	23.83	27.26	27.26	26.05	26.15	27.32	26.18	25.28	28.32
19	24.63	29.40	29.39	27.06	27.41	29.78	28.87	28.05	30.53
20	26.43	31.16	31.27	26.43	26.92	31.25	30.43	29.41	31.55
21	24.24	28.26	28.27	26.66	27.18	28.22	27.45	26.40	29.29
22	24.51	29.03	29.06	26.83	27.64	29.02	27.81	27.18	29.57
23	25.55	32.87	32.75	27.60	23.75	32.58	31.46	30.50	32.34
24	23.85	27.06	27.13	25.86	27.05	27.50	26.63	25.55	28.32
Average	24.57	29.27	29.28	26.69	26.61	29.36	28.43	27.52	30.09

Figure 1. Denoised images of different methods on the image "kodim01" degraded by AWGN with different standard deviations of $\sigma_r = 40$, $\sigma_g = 20$, $\sigma_b = 30$ on R, G, B channels, respectively. The images are better to be zoomed in on screen.

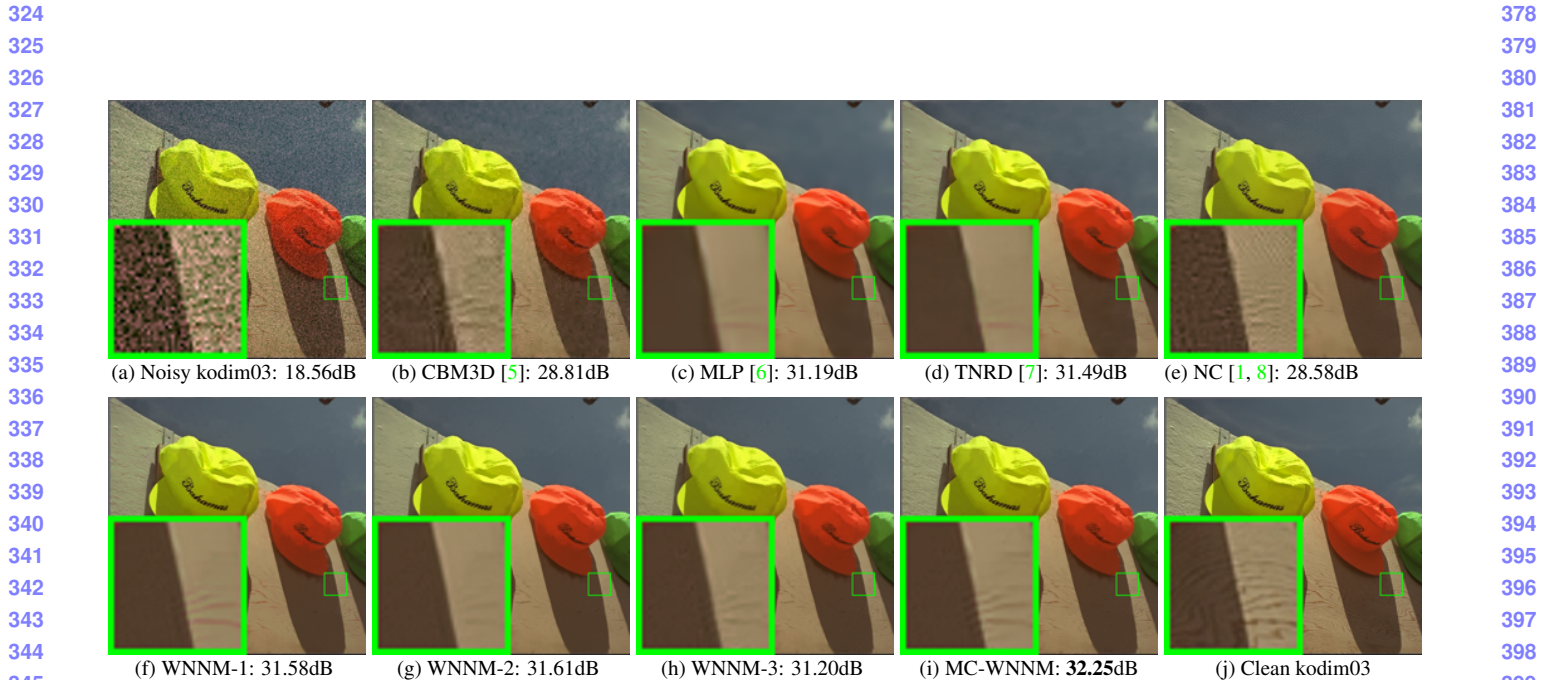


Figure 2. Denoised images of different methods on the image “kodim03” degraded by AWGN with different standard deviations of $\sigma_r = 40$, $\sigma_g = 20$, $\sigma_b = 30$ on R, G, B channels, respectively. The images are better to be zoomed in on screen.

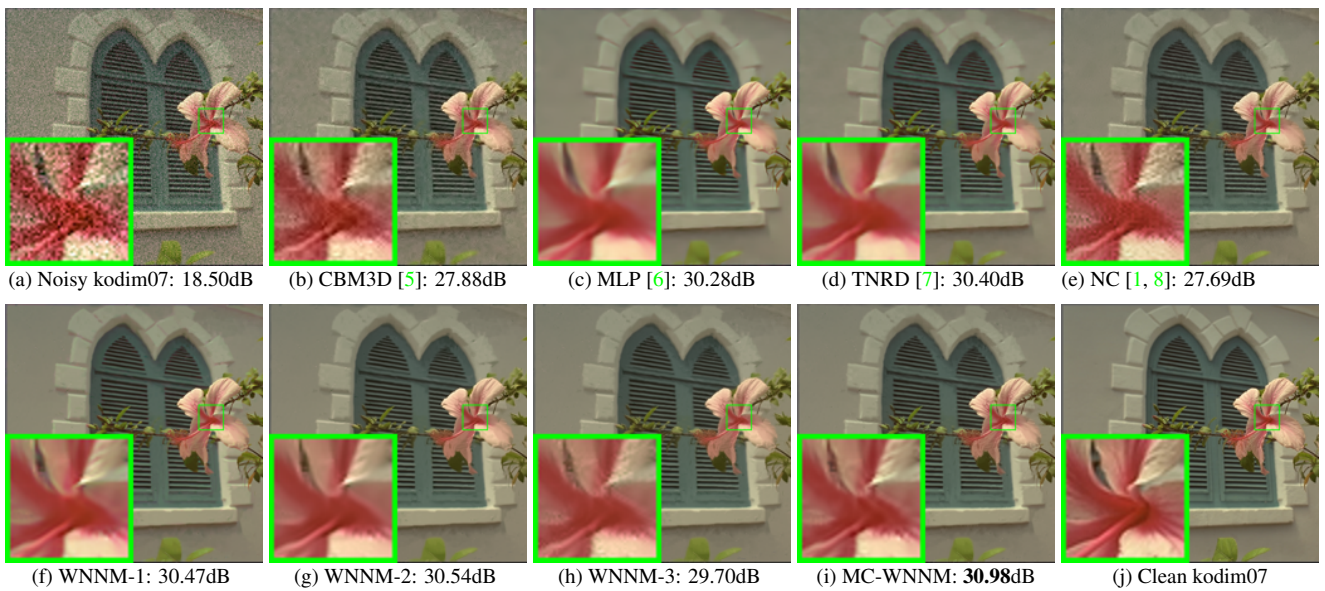


Figure 3. Denoised images of different methods on the image “kodim07” degraded by AWGN with different standard deviations of $\sigma_r = 40$, $\sigma_g = 20$, $\sigma_b = 30$ on R, G, B channels, respectively. The images are better to be zoomed in on screen.

432

433

434

486
487
488

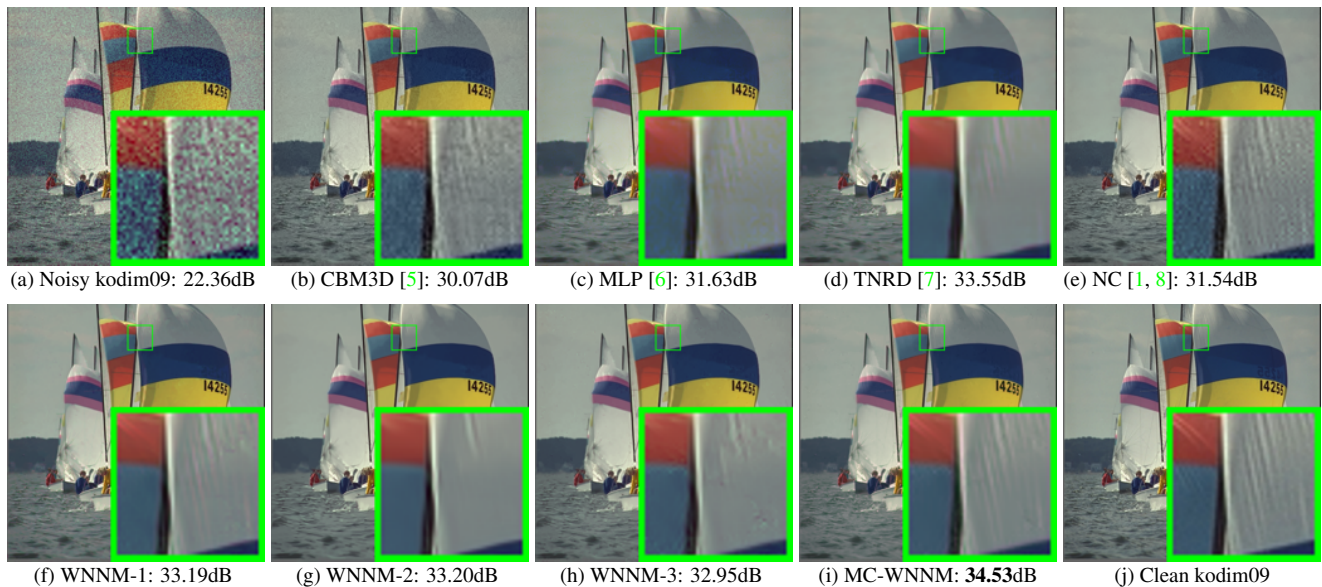


Figure 4. Denoised images of different methods on the image ‘‘kodim09’’ degraded by AWGN with different standard deviations of $\sigma_r = 5, \sigma_g = 30, \sigma_b = 15$ on R, G, B channels, respectively. The images are better to be zoomed in on screen.

456

510

458
459
460
461

512
513
514
515

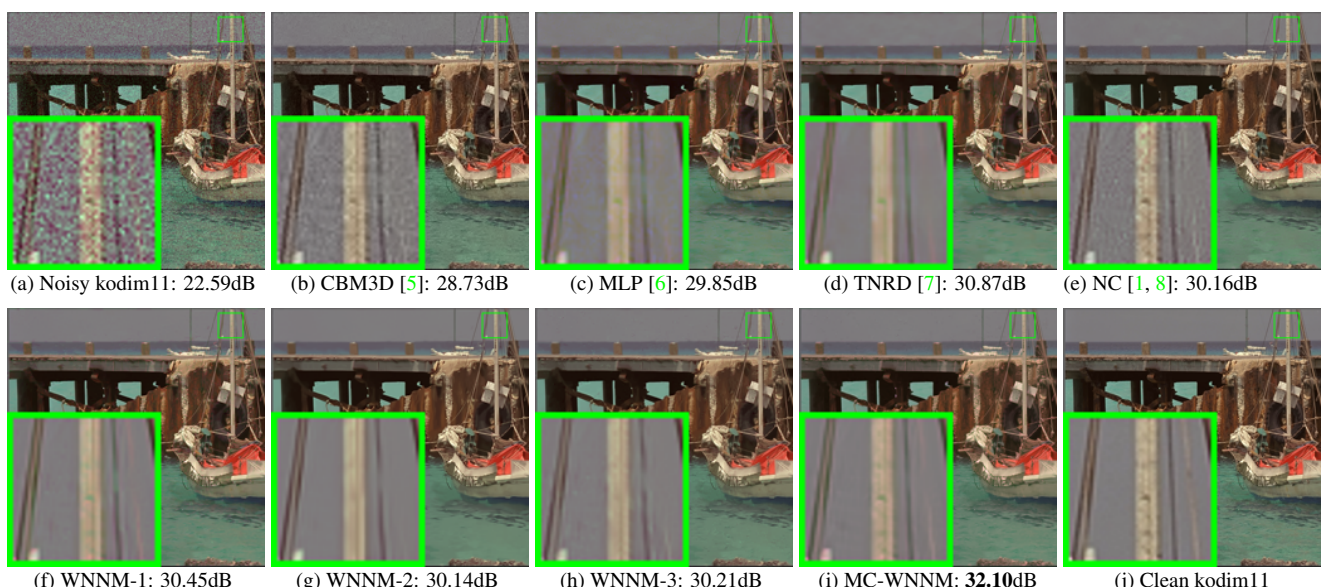
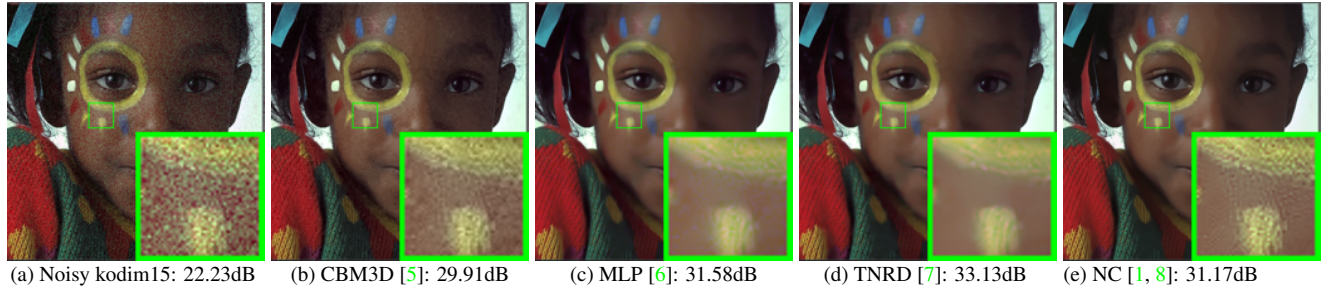


Figure 5. Denoised images of different methods on the image “kodim11” degraded by AWGN with different standard deviations of $\sigma_r = 5$, $\sigma_g = 30$, $\sigma_b = 15$ on R, G, B channels, respectively. The images are better to be zoomed in on screen.

483
484
485

537
538
539

540
541
542594
595
596

543
544
545
546
547
548
549
550
551
552
553
554
555
556
557
558
559
560
561
562
563
564
565
566
567
568
569
570
571
572
573
574
575
576
577
578
579
580
581
582
583
584
585
586
587
588
589
590
591
592
593

(a) Noisy kodim15: 22.23dB (b) CBM3D [5]: 29.91dB (c) MLP [6]: 31.58dB (d) TNRD [7]: 33.13dB (e) NC [1, 8]: 31.17dB
(f) WNNM-1: 33.22dB (g) WNNM-2: 32.34dB (h) WNNM-3: 32.36dB (i) MC-WNNM: 34.27dB (j) Clean kodim15

Figure 6. Denoised images of different methods on the image “kodim15” degraded by AWGN with different standard deviations of $\sigma_r = 5$, $\sigma_g = 30$, $\sigma_b = 15$ on R, G, B channels, respectively. The images are better to be zoomed in on screen.

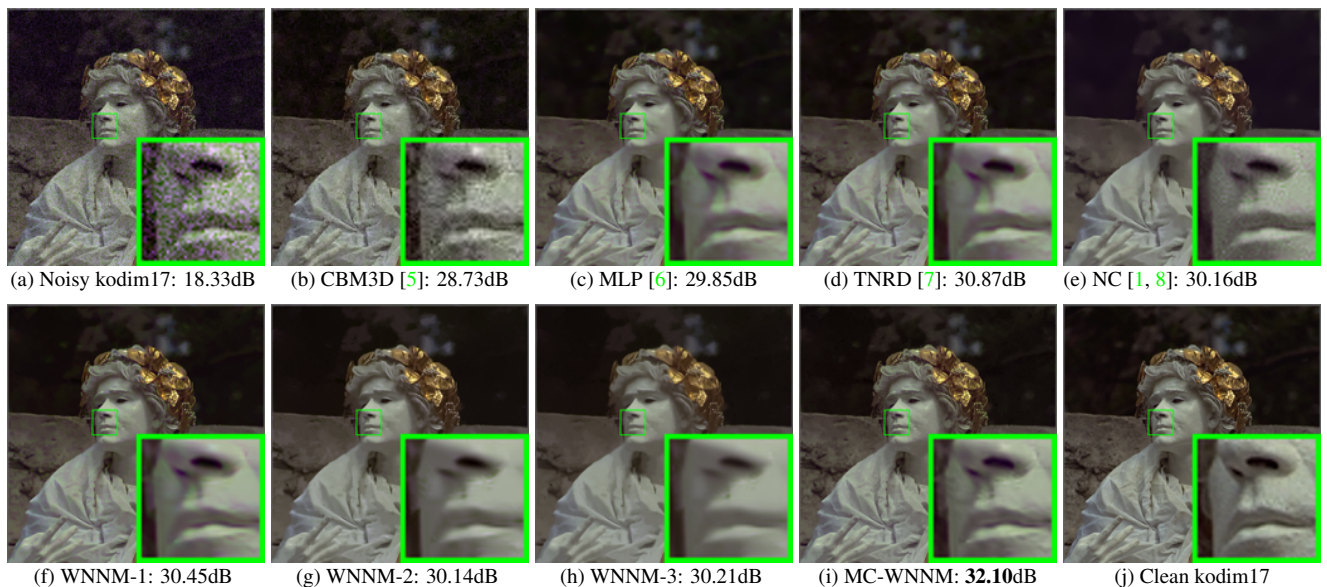
605
606
607
608
609
610
611
612
613
614
615
616
617
618
619
620
621
622
623
624
625
626
627
628
629
630
631
632
633
634
635
636
637
638
639
640
641
642
643
644

Figure 7. Denoised images of different methods on the image “kodim17” degraded by AWGN with different standard deviations of $\sigma_r = 5$, $\sigma_g = 30$, $\sigma_b = 15$ on R, G, B channels, respectively. The images are better to be zoomed in on screen.

645
646
647

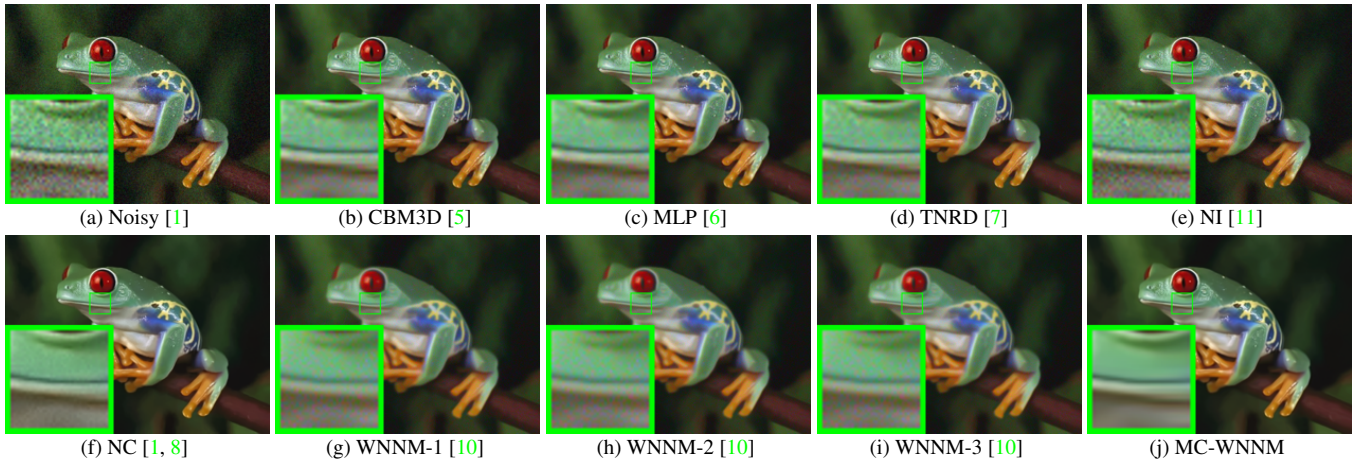


Figure 8. Denoised images of the real noisy image “Frog” [1] by different methods. The images are better to be zoomed in on screen.

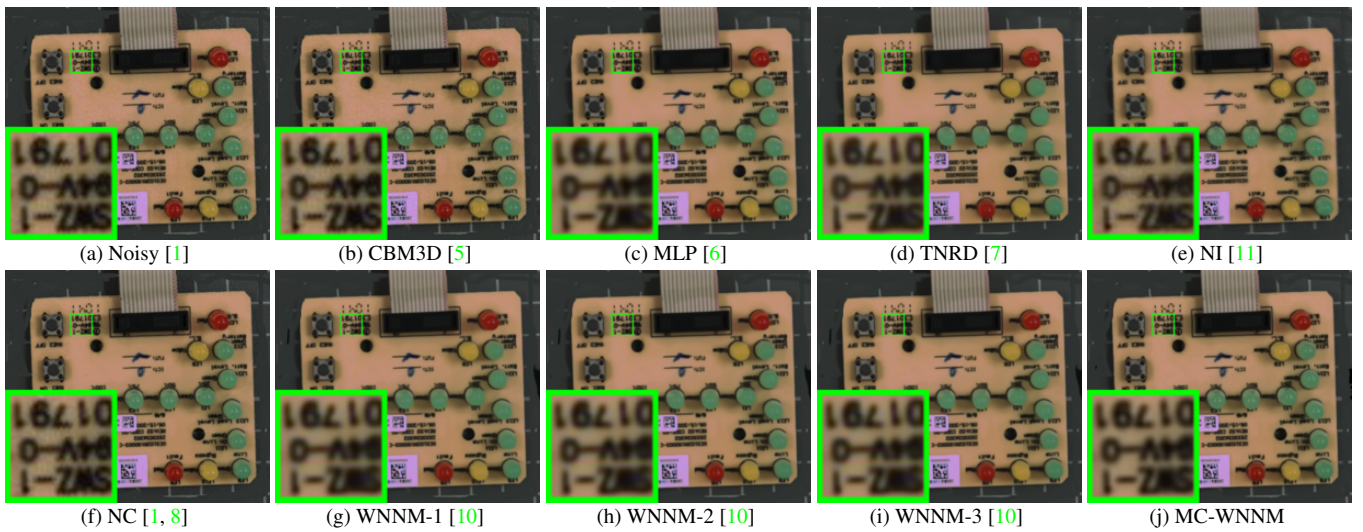


Figure 9. Denoised images of the real noisy image “Circuit” [1] by different methods. The images are better to be zoomed in on screen.

683 3. More visual comparisons of denoised images by different methods on the real noisy images of 684 the dataset [1]

686 In this section, we give more comparisons of the state-of-the-art denoising methods on the dataset [1]. The real noisy
687 images in dataset [1] have no “ground truth” images and hence we only compare the visual quality of the denoised images by
688 different methods. As can be seen from Figures ??-??, our proposed method performs better than the competing methods.
689

690 4. More visual comparisons of denoised images by different methods on the real noisy images of 691 the dataset [2]

693 In this section, we provide more comparisons of the proposed method with the state-of-the-art denoising methods on the
694 15 cropped real noisy images used in [2]. In this dataset, each scene was shot 500 times under the same camera and camera
695 setting. The mean image of the 500 shots is roughly taken as the “ground truth”, with which the PSNR can be computed.
696 As can be seen from Figures 16-??, in most cases, our proposed method achieves better performance than the the competing
697 methods. This validates the effectiveness of our proposed external prior guided internal prior learning framework for real
698 noisy image denoising.
699

756

810

757

811

758

812

759

813

760

814

761

815

762

816

763

817

764

818

765

819

766

820

767

821

768

822

769

823

770

824

771

825

772

826

773

827

774

828

775

829

776

830

777

831

778

832

779

833

780

834

781

835

782

836

783

837

784

838

785

839

786

840

787

841

788

842

789

843

790

844

791

845

792

846

793

847

794

848

795

849

796

850

797

851

798

852

799

853

800

854

801

855

802

856

803

857

804

858

805

859

806

860

807

861

808

862

809

863

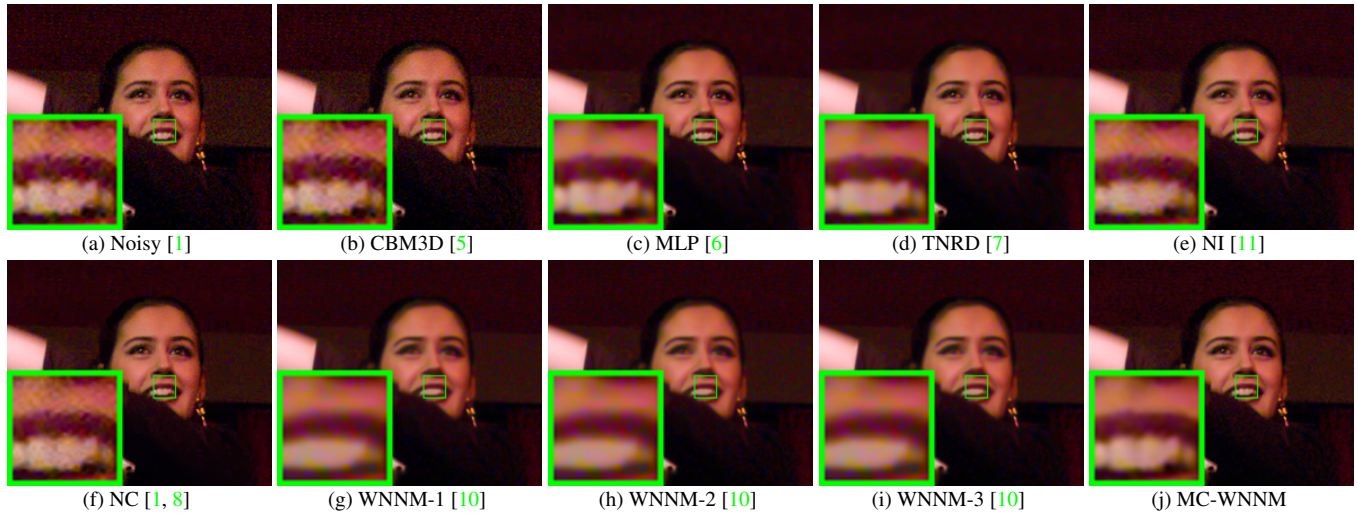


Figure 10. Denoised images of the real noisy image “Woman” [1] by different methods. The images are better to be zoomed in on screen.

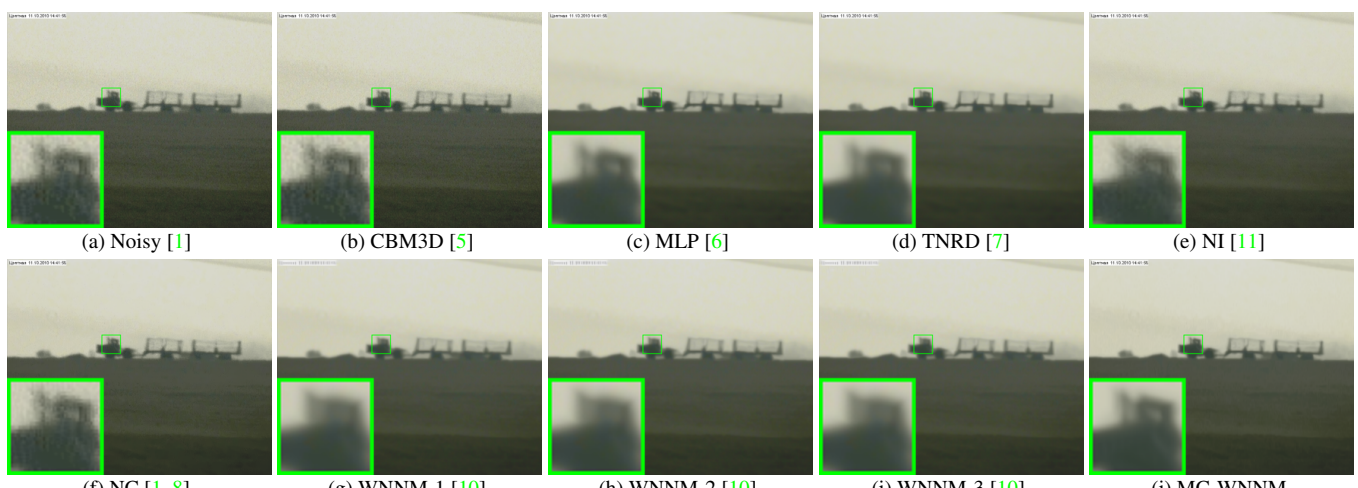


Figure 11. Denoised images of the real noisy image “Vehicle” [1] by different methods. The images are better to be zoomed in on screen.

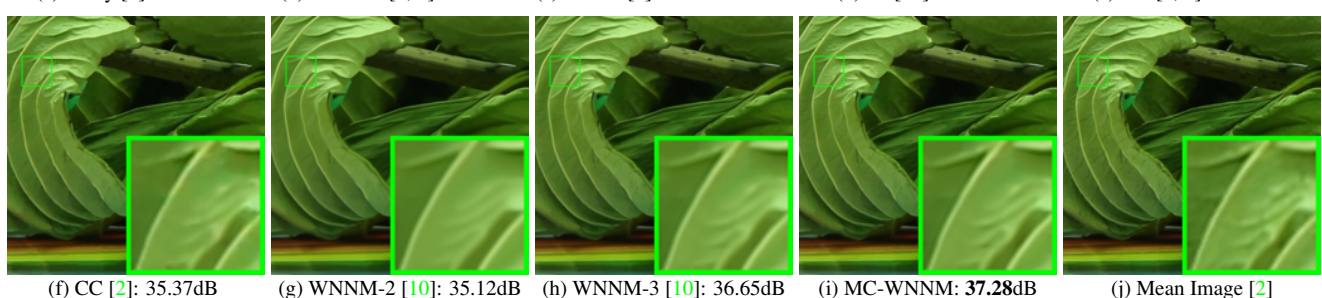
864
865
866
867918
919
920
921
922
923
924
925
926
927
928
929
930931
932
933
934
935
936
937
938
939

Figure 12. Denoised images of a region cropped from the real noisy image “Canon 5D Mark 3 ISO 3200 2” [2] by different methods. The images are better to be zoomed in on screen.

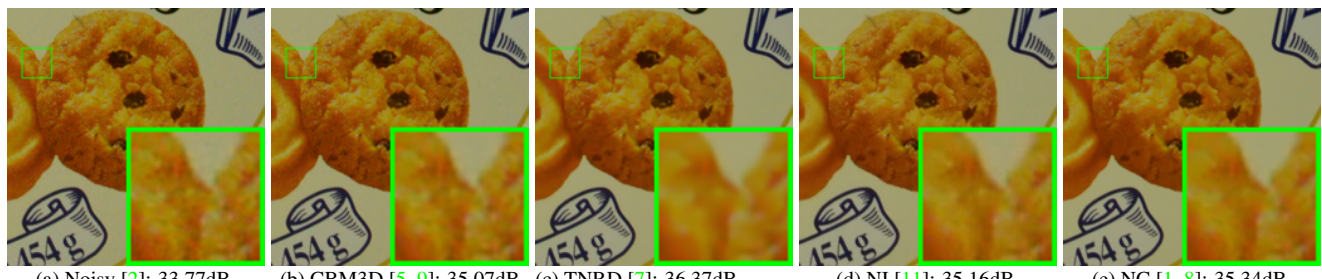
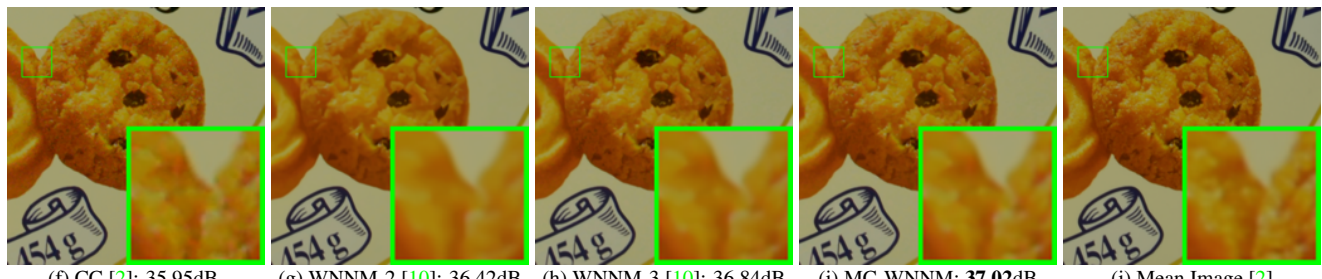
888
889
890
891
892
893
894940
941
942
943
944
945
946
947
948
949
950
951
952
953
954
955
956
957958
959
960
961
962
963
964
965
966
967
968
969
970
971

Figure 13. Denoised images of a region cropped from the real noisy image “Nikon D600 ISO 3200 2” [2] by different methods. The images are better to be zoomed in on screen.

915
916
917

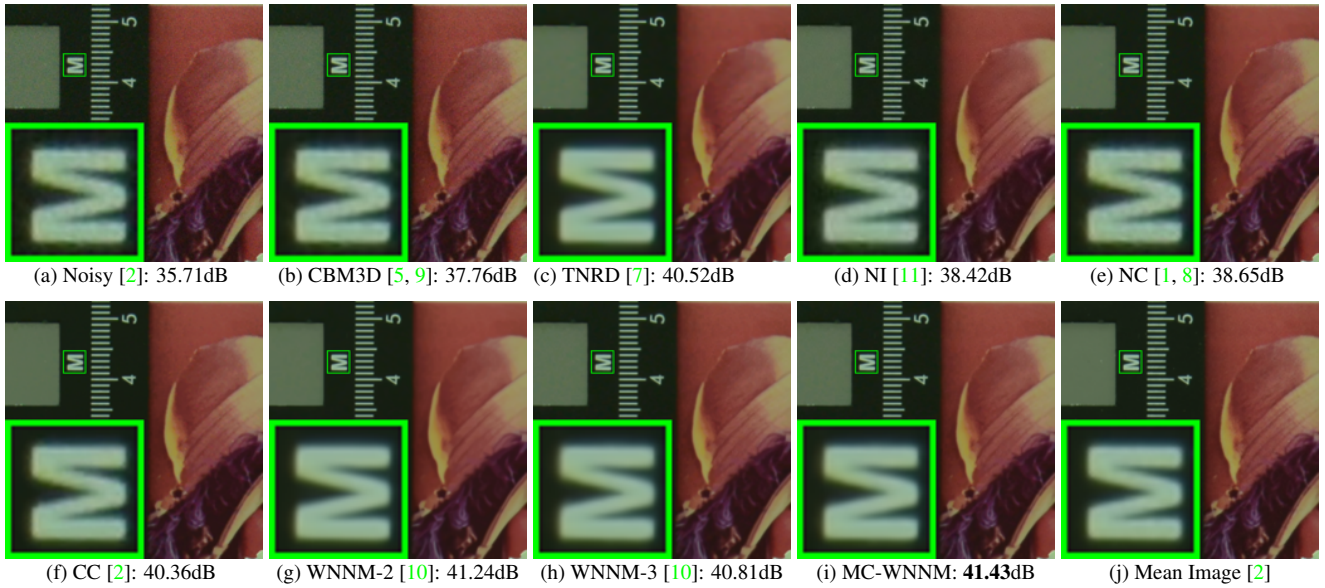


Figure 14. Denoised images of a region cropped from the real noisy image “Nikon D800 ISO 1600 2” [2] by different methods. The images are better to be zoomed in on screen.

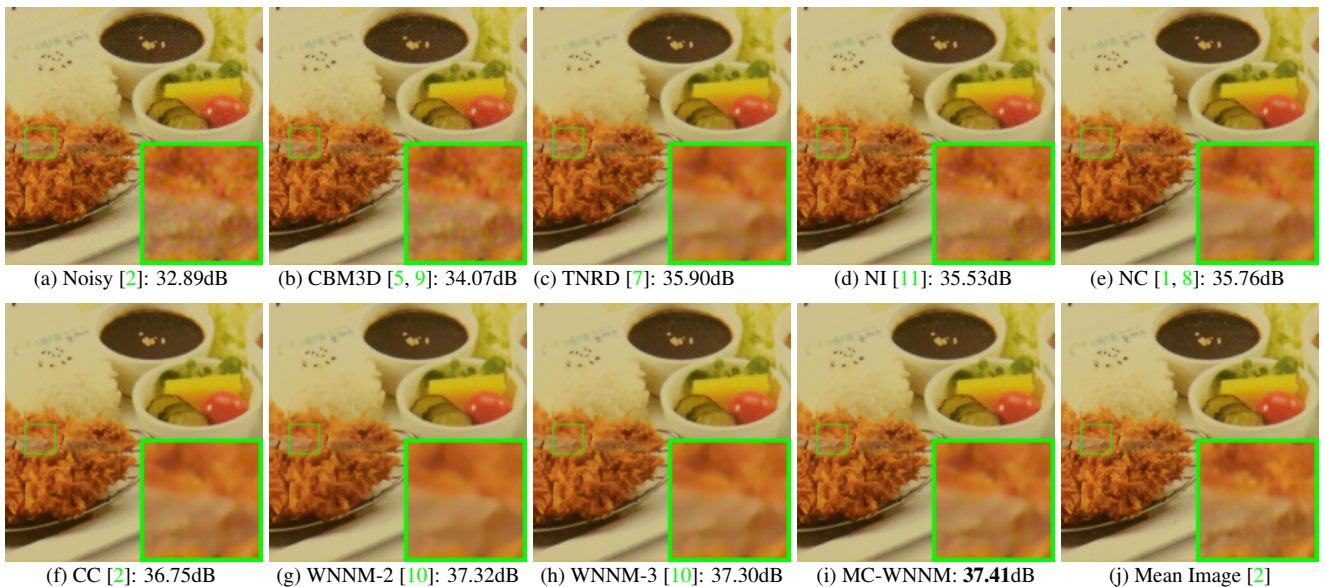


Figure 15. Denoised images of a region cropped from the real noisy image “Nikon D800 ISO 3200 2” [2] by different methods. The images are better to be zoomed in on screen.

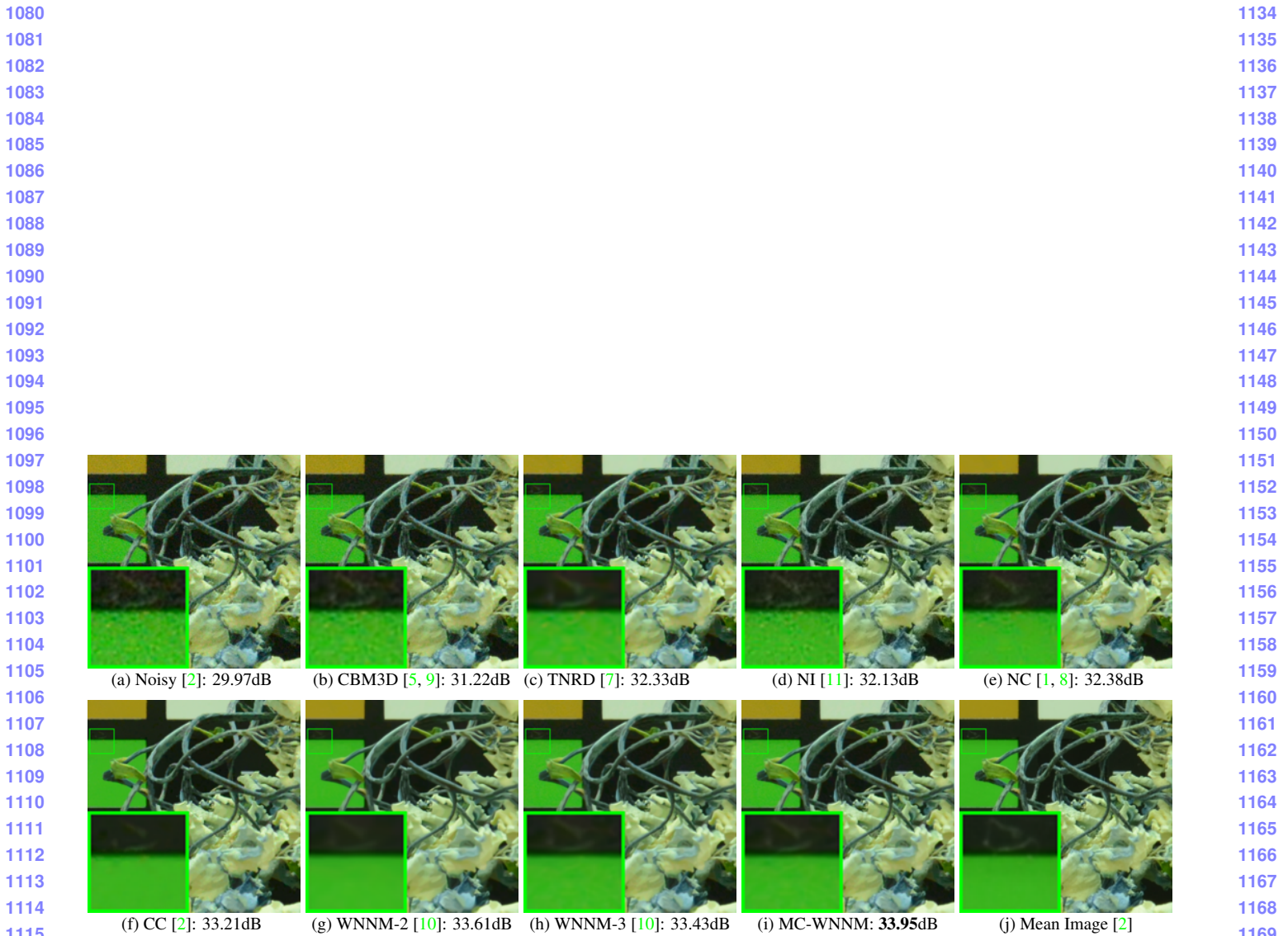


Figure 16. Denoised images of a region cropped from the real noisy image “Nikon D800 ISO 6400 2” [2] by different methods. The images are better to be zoomed in on screen.

1188	References	1242
1189		1243
1190	[1] M. Lebrun, M. Colom, and J. M. Morel. The noise clinic: a blind image denoising algorithm. http://www.ipol.im/pub/ art/2015/125/ . Accessed 01 28, 2015. 1, 3, 4, 5, 6, 7, 8, 9, 10, 11	1244
1191		1245
1192	[2] S. Nam, Y. Hwang, Y. Matsushita, and S. J. Kim. A holistic approach to cross-channel image noise modeling and its application to image denoising. <i>IEEE Conference on Computer Vision and Pattern Recognition (CVPR)</i> , pages 1683–1691, 2016. 1, 7, 9, 10, 11	1246
1193		1247
1194	[3] C. Eckart and G. Young. The approximation of one matrix by another of lower rank. <i>Psychometrika</i> , 1(3):211–218, 1936. 1	1248
1195		1249
1196	[4] S. Gu, Q. Xie, D. Meng, W. Zuo, X. Feng, and L. Zhang. Weighted nuclear norm minimization and its applications to low level vision. <i>International Journal of Computer Vision</i> , pages 1–26, 2016. 1	1250
1197		1251
1198	[5] K. Dabov, A. Foi, V. Katkovnik, and K. Egiazarian. Color image denoising via sparse 3D collaborative filtering with grouping constraint in luminance-chrominance space. <i>IEEE International Conference on Image Processing (ICIP)</i> , pages 313–316, 2007. 3, 4, 5, 6, 7, 8, 9, 10, 11	1252
1199		1253
1200	[6] H. C. Burger, C. J. Schuler, and S. Harmeling. Image denoising: Can plain neural networks compete with BM3D? <i>IEEE Conference on Computer Vision and Pattern Recognition (CVPR)</i> , pages 2392–2399, 2012. 3, 4, 5, 6, 7, 8	1254
1201		1255
1202	[7] Y. Chen, W. Yu, and T. Pock. On learning optimized reaction diffusion processes for effective image restoration. <i>IEEE Conference on Computer Vision and Pattern Recognition (CVPR)</i> , pages 5261–5269, 2015. 3, 4, 5, 6, 7, 8, 9, 10, 11	1256
1203		1257
1204	[8] M. Lebrun, M. Colom, and J.-M. Morel. Multiscale image blind denoising. <i>IEEE Transactions on Image Processing</i> , 24(10):3149– 3161, 2015. 3, 4, 5, 6, 7, 8, 9, 10, 11	1258
1205		1259
1206	[9] K. Dabov, A. Foi, V. Katkovnik, and K. Egiazarian. Image denoising by sparse 3-D transform-domain collaborative filtering. <i>IEEE Transactions on Image Processing</i> , 16(8):2080–2095, 2007. 9, 10, 11	1260
1207		1261
1208	[10] S. Gu, L. Zhang, W. Zuo, and X. Feng. Weighted nuclear norm minimization with application to image denoising. <i>IEEE Conference on Computer Vision and Pattern Recognition (CVPR)</i> , pages 2862–2869, 2014. 7, 8, 9, 10, 11	1262
1209		1263
1210	[11] Neatlab ABSoft. Neat Image. https://ni.neatvideo.com/home . 7, 8, 9, 10, 11	1264
1211		1265
1212		1266
1213		1267
1214		1268
1215		1269
1216		1270
1217		1271
1218		1272
1219		1273
1220		1274
1221		1275
1222		1276
1223		1277
1224		1278
1225		1279
1226		1280
1227		1281
1228		1282
1229		1283
1230		1284
1231		1285
1232		1286
1233		1287
1234		1288
1235		1289
1236		1290
1237		1291
1238		1292
1239		1293
1240		1294
1241		1295